J Appl Electrochem (2014) 44:419–425
DOI 10.1007/s10800-013-0645-z

ORIGINAL ARTICLE

Electrochemical determination of dissolved oxygen based on three dimensional electrosynthesis of silver nanodendrites electrode

Di Zhang · Yuxin Fang · Zhiying Miao · Min Ma · Qiang Chen

Received: 16 September 2013 / Accepted: 18 November 2013 / Published online: 29 November 2013

Abstract In this paper, a highly sensitive electrochemical sensor for dissolved oxygen was prepared. A glassy carbon electrode was modified with silver nanodendrites that were synthesized by electrochemical deposition on the electrode without the use of a surfactant or template. The electrode displayed efficient electrocatalytic reduction of dissolved oxygen to form hydroxy ions via a four-electron reduction pathway, and a significant decrease in the respective overvoltage. The sensor responded linearly to dissolved oxygen in the 1.0–66.7 μM concentration range, and had a remarkably good sensitivity (0.169 μA μM^{-1}) at an applied potential of −300 mV (vs. Ag/AgCl). The lower detection limit was 0.043 μM (at the signal-to-noise ratio of 3), and the response time was 5 s. The good performance was attributed to the enlarged electro-active surface of the dendritic silver nanostructures and to the efficiency of electron transfer between dissolved oxygen and the electrode. The sensor also showed good reproducibility, long-term stability, and relative good selectivity.

Keywords Dissolved oxygen detection · Silver nanodendrites · Electrocatalysis · Oxygen sensor

D. Zhang · Z. Miao · M. Ma · Q. Chen (✉)
The Key Laboratory of Bioactive Materials, Ministry of Education, College of Life Science, Nankai University, Weijin Road No. 94, Tianjin 300071, People's Republic of China
e-mail: qiangchen@nankai.edu.cn

Y. Fang
College of Acupuncture and Moxibustion, Tianjin University of Traditional Chinese Medicine, Tianjin 300193, People's Republic of China

1 Introduction

Oxygen reduction reaction has been of great importance in many processes, such as in fuel cells, neuroscience, many biological processes, and chemical synthesis [1–3]. Therefore, the detection of dissolved oxygen in aqueous solutions is an essential task. Different detection systems such as colorimetry [4], fluorescence [5], and chemiluminescence [6] have been proposed for this purpose. Since the introduction of Clark-type sensor [7], electrochemical protocol has been widely applied for the dissolved oxygen measurement because of its high sensitivity and selectivity.

However, direct dissolved oxygen reduction at solid electrode is a slow kinetics process and needs a high potential, so more and more researchers pay attention to studying electrocatalytic reactions of oxygen. Several electrocatalytic materials have been used to improve the electrons transfer efficiency between dissolved oxygen and electrode surface, such as nickel-salen polymeric film [8], porphyrins complexes [9], SiO_2/SnO_2/manganese(II) phthalocyanine [10], palladium [11], cobalt complexes [12], carbon nanotube [13, 14], gold nanoparticles [15], nano-platinum [16–18], and so on. Recently, as a typical nanomaterial, silver nanostructures are also studied as cathode electroreduction for dissolved oxygen. Kongkanand and Kuwabata [19] reported that oxygen reduction occured at silver monolayer islands deposited on gold substrate, Demarconnay et al. [20] prepared the Ag/C catalysts for dioxygen electroreduction, and Lu et al. [21] proposed the silver nanorods for oxygen reduction. The above studies all indicated that silver nanomaterials exhibited catalytic activity for the reduction of dissolved oxygen. However, most of previous reports were focused on the nanoparticles or one-dimensional nanostructures, there are few studies about three-dimensional silver

nanomaterials for oxygen electroreduction. As is well known, different morphologies of metal nanomaterials can affect the electrocatalytic behavior [22]. So it is necessary to research the performance of three-dimensional silver nanostructures on dissolved oxygen reduction.

The aim of the present work was to prepare a sensitive dissolved oxygen sensor based on three-dimensional silver nanodendrites obtained by electrodeposition on a bare GC electrode without additional chemical reagent or irradiation. The resulted nanomaterials were characterized by various analysis tools. The electrocatalytic activity for dissolved oxygen was compared with that of analogous bare Ag and GC electrode, and the mechanism of the electrocatalytic reduction of dissolved oxygen on the silver dendrites modified electrode was studied.

2 Experimental

2.1 Reagents and materials

Silver nitrate ($AgNO_3$) was purchased from Tianjin Yingda Rare Chemical Reagent Co. Potassium nitrate (KNO_3) was obtained from Tianjin University, Tianjin Chemical Experiment Plant. All solutions used in this study were of analytical grade, and doubly distilled water was used throughout. Freshly prepared 0.1 M phosphate buffer solution (PBS, pH 7.0), consisting of Na_2HPO_4 and KH_2PO_4, was used as the supporting electrolyte. The O_2-saturated standard solution was produced by bubbling PBS with pure O_2 for 30 min, in which the dissolved oxygen content was 2.6×10^{-4} M calculated from its saturated solubility [23]. All experiments were performed at room temperature, $\sim$25 °C.

2.2 Apparatus

The electrochemical measurements were carried out in a conventional one-compartment cell using a 283 Potentiostat–Galvanostat electrochemical workstation (EG&G PARC with M270 software). A conventional three-electrode system, containing the Ag nanodendrites modified GC electrode (3 mm diameter) as a working electrode, a platinum wire (1 mm diameter) as a counter electrode, and an Ag/AgCl electrode (saturated with KCl) as a reference electrode was employed for all electrochemical experiments.

The X-ray diffraction (XRD) pattern was recorded using a Rigaku D/max rA with Cu Kα radiation ($\lambda = 1.5418$ Å) on a diffractometer (Rigaku, Japan). A scan rate of 4° min^{-1} was applied to record the pattern in the 2θ range 30°–80°. Scanning electron microscopy (SEM) was performed using a field emission microscope (QUANTA 200, FEI Co.). Transmission electron microscopy (TEM) image was obtained by using Tecnai G2 F20 instrument (Philips Holland) equipped with an energy-dispersive X-ray spectroscopy (EDX) analyzer.

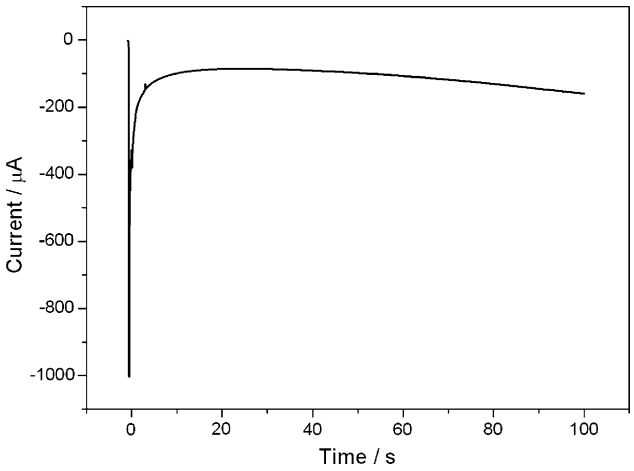

Fig. 1 *I-t* curve for the electrodeposition of silver in 0.1 M KNO_3 solution containing 15 mM $AgNO_3$

2.3 Preparation of the dendritic silver nanostructures modified GC electrode

The bare GC electrode was polished with 0.3 and 0.05 μm aluminum oxide slurries, respectively, and ultrasonically cleaned with ethanol and double distilled water for 10 min to remove the physically adsorbed substances. According to the method reported in previous article [24] of our group with slight modifications, the silver nanodendrites were synthesized by chronoamperometry electrodeposited onto the GC electrode in a 0.1 M KNO_3 solution containing 15 mM $AgNO_3$ by applying a potential step of −300 mV for 100 s.

3 Results and discussion

3.1 Electrochemical deposition of silver nanodendrites

The typical current *vs* time curve as the electrochemical deposition process was presented in Fig. 1. From the curve, silver ions were reduced to silver atoms ($Ag^+ + e^- \rightarrow Ag$) under the negative potential of −300 mV in the solution containing 15 mM $AgNO_3$ and 0.1 M KNO_3, and then deposited on the GC electrode. Silver atoms accumulated on the electrode surface as time goes on.

3.2 Morphology and characterization of the dendritic silver nanostructures

Figure 2 shows the typical SEM and TEM images of silver dendrites. As can be seen from the SEM image (Fig. 2a),

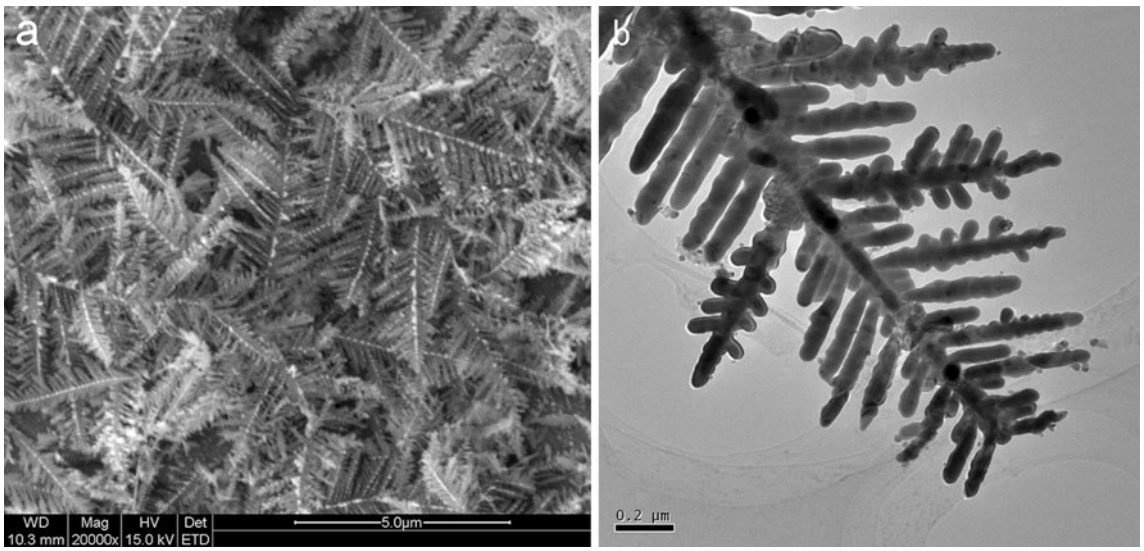

Fig. 2 SEM image (**a**) and TEM image (**b**) of silver dendrites

over 95 % of the products are elegant dendrites. And each silver dendrite is made up of a long central trunk and secondary or tertiary branches. The further detailed examination from the TEM image in Fig. 2b shows that angles between the trunk and the branches are fixed at about 60°, indicating the growth of the dendrites may be locally controlled by the oriented attachment [25].

The composition of typical silver nanodendrites was further probed by EDX analysis (Fig. 3a), which reveals that there is no residual impurity in the product. The strong signals from the Ag atoms are observed, while the peaks of Cu and C in the spectrum should be from the substrate. The XRD patterns were further used to examine the crystal structure of the sample in Fig. 3b. The four diffraction peaks can be indexed to the (111), (200), (220), and (311) planes of high crystallinity and the face centered cubic (fcc) structure of silver [26]. The above research results were consistent with previous report obtained by our group.

3.3 Electrochemical behavior of the silver dendrites modified GC electrode toward the dissolved oxygen

The electrochemical response of the silver dendrites modified GC electrode to the dissolved oxygen was investigated. Figure 4 shows the cyclic voltammograms of the bare GC electrode (A), the bare Ag electrode (B) and the silver nanodedrites modified GC electrode (C) in pH 7.0 N_2-saturated PBS (a) and O_2-saturated PBS (b). Firstly, from the CV of the bare GC electrode (curve a, Fig. 4A), the bare Ag electrode (curve a, Fig. 4B) and the silver nanodedrites modified GC electrode (curve a, Fig. 4C) in N_2-saturated solution, the voltammetric currents are featureless and no reduction peaks are observed in the scan range. In contrast, in O_2-saturated PBS the dissolved oxygen reduction peaks in different sizes and shapes are observed. Besides, there is virtually no current in the anodic sweep, as expected for a totally irreversible process.

Secondly, the oxygen reduction on the bare Ag electrode presents two small cathodic peaks (curve b, Fig. 4B), it can be probably attributed to the 2-step four-electron reduction of dissolved oxygen in neutral conditions [27], i.e., the first reduction peak at −422 mV is due to the reduction of O_2 to H_2O_2 and OH^- as:

$$O_2 + 2H_2O + 2e^- \rightarrow H_2O_2 + 2OH^- \quad (1)$$

While the second reduction peak of H_2O_2 to OH^- at −778 mV takes place as:

$$H_2O_2 + 2e^- \rightarrow 2OH^- \quad (2)$$

And from the Fig. 4C, only one sharp cathodic peak appears for silver deposited electrode at −330 mV (curve b). Such voltammetric feature strongly reflects that the fast and efficient four-electron reaction of dissolved oxygen reduction occurred on silver nanodendrites modified GC electrode as:

$$O_2 + 2H_2O + 4e^- \rightarrow 4OH^- \quad (3)$$

This mechanism of four-electron process toward dissolved oxygen reduction is consistent with that at other silver nanostructures modified electrode reported previously [19, 21].

Moreover, as can be seen in Fig. 4C (b), the increase of the peak current and the positive shift of the potential indicates that the three-dimensional silver dendrites modified electrode have the larger active surface area

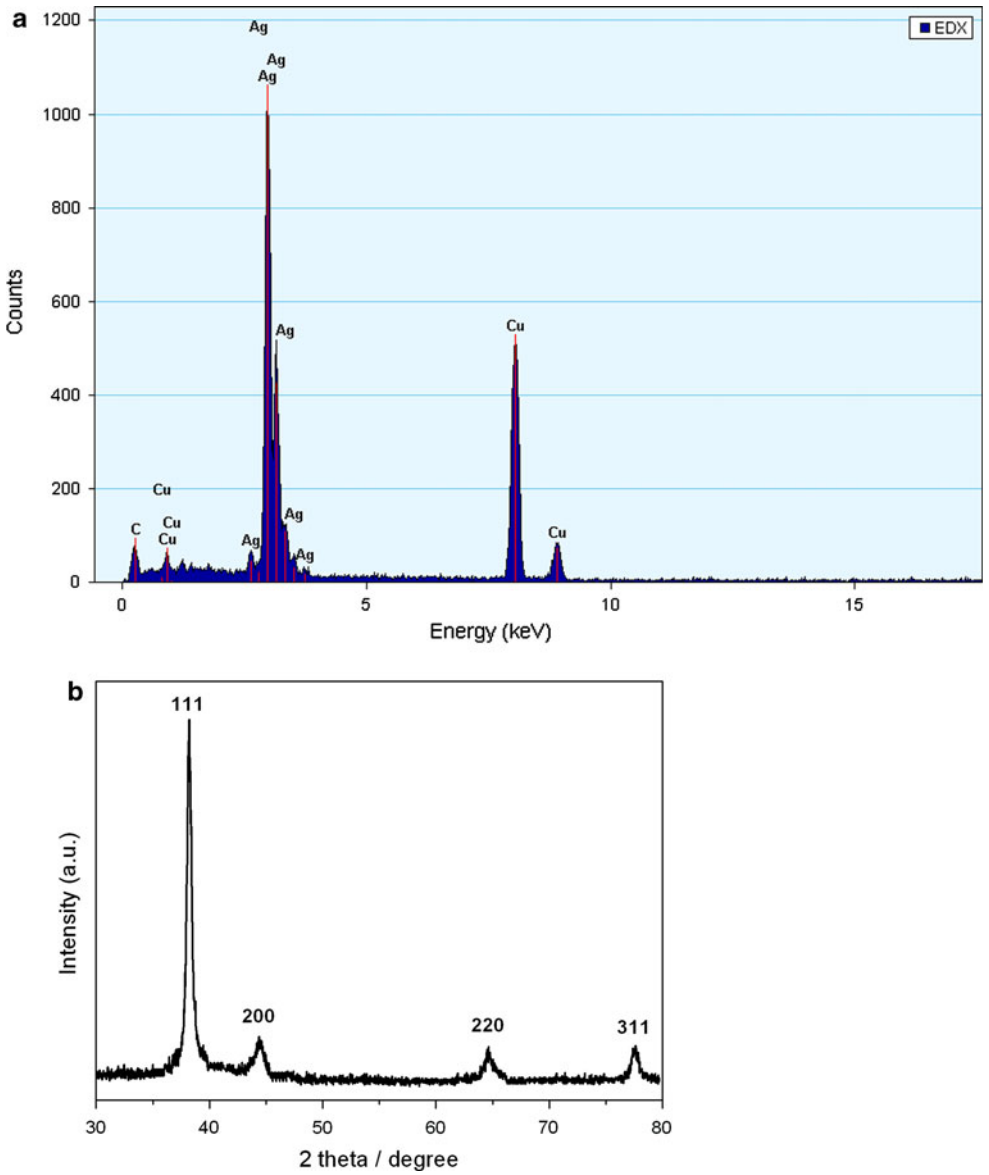

Fig. 3 **a** EDX spectrum of dendritic silver nanostructures dropped on a cupper pillar, **b** XRD pattern of as-prepared silver nanodendrites

and better catalytic activity to the electrochemical reduction of dissolved oxygen than the bare GC or Ag electrode.

The catalytic activity of as-prepared sensor for various dissolved oxygen concentration was examined in Fig. 5. It is found that the electrocatalytic current gradually increased with the increment of dissolved oxygen concentration (from the top: 1, 6.22, 13.18, 21.57, and 29.7 μM).

Furthermore, the electrocatalytic behavior of the as-prepared electrode to dissolved oxygen was studied with the change of scan rate. As shown in Fig. 6a, with the increasing of the sweep rate from 10 to 125 mV s^{-1}, the cathodic peak current of dissolved oxygen increases and the peak potential shifts to more negative position. And from the Fig. 6b, the reduction peak current (I_p) increases linearly with the square root of the sweep rate ($\upsilon^{1/2}$), indicating that the reduction process of the electrode reaction is diffusion controlled, which is in accordance with the Andrieux and Savéant theoretical model [28], I_p is proportional to the $\upsilon^{1/2}$ as follows:

$$I_p = 0.496nFAC_sD_s^{1/2}\upsilon^{1/2}(nF/RT)^{1/2} \quad (4)$$

where n, F, A, C_s, Ds, R, and T are constant values.

As we known, the pH of the solution plays an important part in the detection of dissolved oxygen. The effect of pH on cathodic peak current of dissolved oxygen was realized in 0.1 M PBS with pH 5.5, 6.0, 6.5, 7.0, 7.5, and 8.0

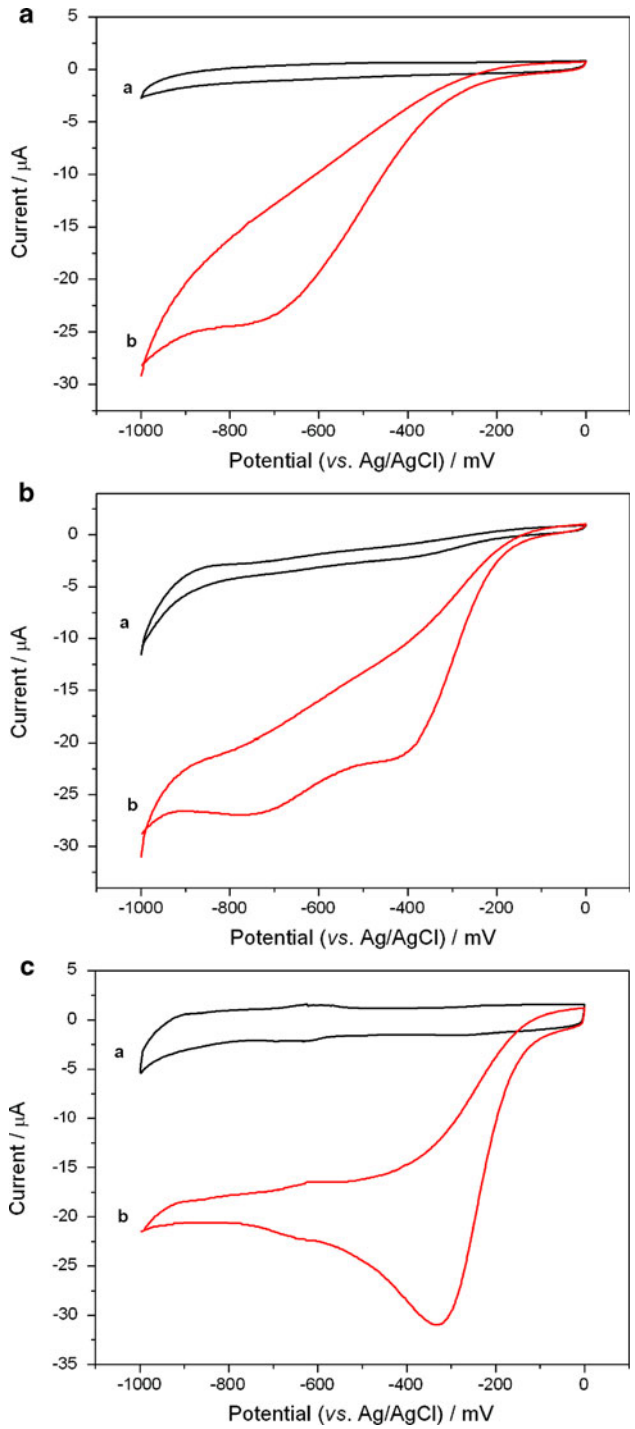

Fig. 4 Cyclic voltammograms of the bare GC electrode (**A**), the bare Ag electrode (**B**) and the silver nanodedrites modified GC electrode (**C**) in pH 7.0 N_2-saturated PBS (*a*) and O_2-saturated PBS (*b*). Scan rate: 50 mV s^{-1}

(Fig. 7). One can notice that the current responses increased with the increase of solution pH from 5.5 to 7.0 and decreased thereafter. So in order to obtain optimized condition, a PBS of pH 7.0 was used to control the solution pH in subsequent experiments.

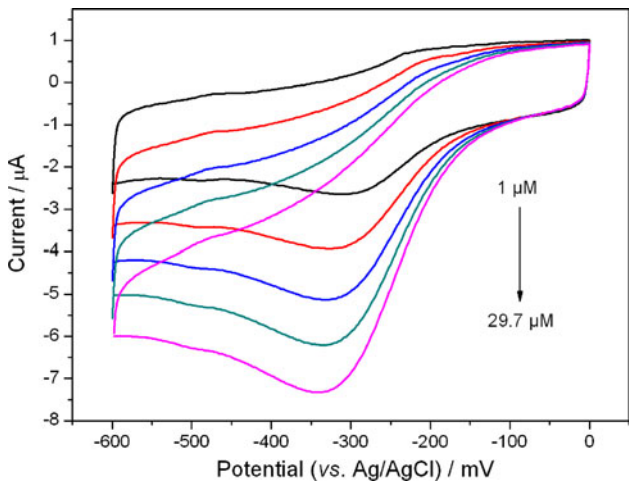

Fig. 5 Cyclic voltammograms of silver dendrites modified GC electrode in PBS solution (pH 7.0) for different dissolved oxygen concentrations (from the *top* 1, 6.22, 13.18, 21.57, and 29.7 μM). Scan rate: 50 mV s^{-1}

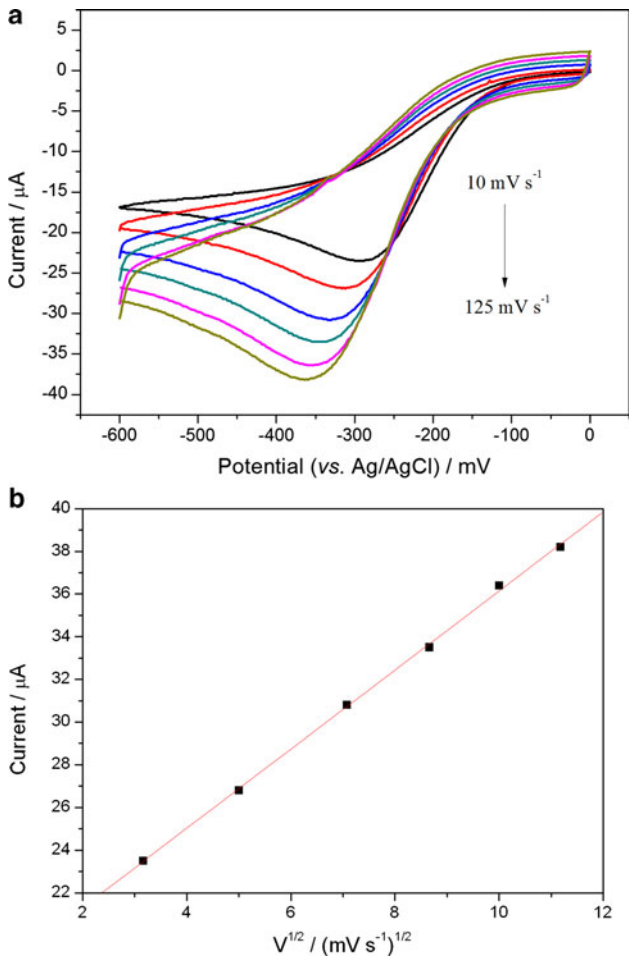

Fig. 6 **a** Cyclic voltammograms of silver dendrites modified electrode in O_2-saturated PBS (pH 7.0) at different scan rate. (From the *top* 10, 25, 50, 75, 100, and 125 mV s^{-1}). **b** The linearity of the currents with the square root of scan rate

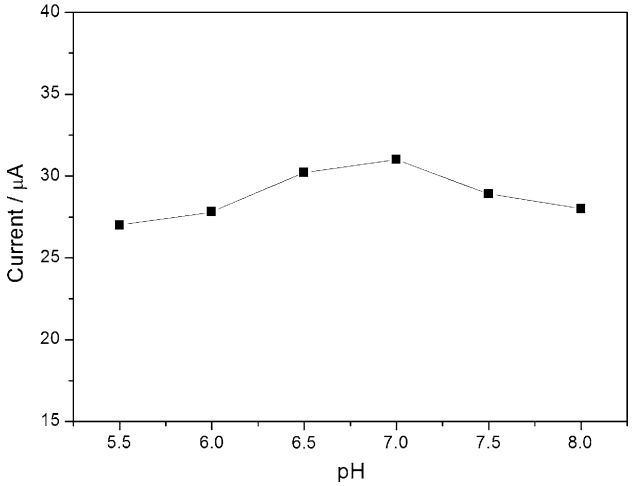

Fig. 7 The influence of pH on the cathodic peak current for dissolved oxygen reduction in O_2-saturated PBS (scan rate: 50 mV s^{-1})

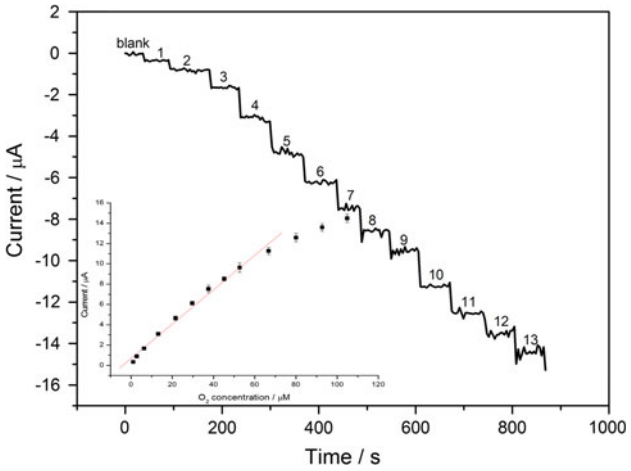

Fig. 8 Amperometric response for the reduction of dissolved oxygen on the silver dendrites modified electrode at concentrations of: (*1*) 1 μM, (*2*) 2.74 μM, (*3*) 6.22 μM, (*4*) 13.18 μM, (*5*) 21.57 μM, (*6*) 29.7 μM, (*7*) 37.58 μM, (*8*) 45.23 μM, (*9*) 52.66 μM, (*10*) 66.71 μM, (*11*) 80.04 μM, (*12*) 92.72 μM, and (*13*) 104.81 μM. Applied potential: −300 mV. *Inset* linear calibration curve

3.4 Determination of dissolved oxygen

To determine the concentration of dissolved oxygen, amperometric measurement was performed in a stirred PBS (pH 7.0) at an applied potential of −300 mV. The experimental solution was deaerated by highly pure nitrogen for 30 min before testing. Figure 8 shows the amperometric response of the Ag/GC electrode to the successive addition of dissolved oxygen at different concentration. The trace reveals that the modified electrode responds rapidly to successive addition of different concentration of dissolved oxygen, reaching a steady-state value within 5 s (achieving 95 % of the steady-state current). The inset of Fig. 8 shows the calibration curve of the dissolved oxygen sensor. The linear response was proportional to the dissolved oxygen concentration in the range from 1.0 to 66.71 μM with a correlation coefficient of 0.995. The sensitivity was 0.169 μA μM^{-1}, which was higher than that at a gold nanoparticles/multi-walled carbon nanotubes-iron picket-fence porphyrin modified electrode (0.0594 μA μM^{-1}) [14] and a SiO_2/SnO_2/Manganese (II) phthalocyanine electrode (0.147 μA μM^{-1}) [10]. In addition, the detection limit was 0.043 μM at the signal-to-noise ratio of 3, which was much lower than 1.156 μM at poly(methylene blue) doped silica nanocomposites modified electrode [29], 0.625 μM at layer-by-layer assembly host-guest supramolecular modified electrode [30] and 3 μM at cobalt tetrasulphonated phthalocyanine/poly-L-lysine film electrode [31]. It can be seen that the proposed sensor exhibited a good performance than other reported dissolved oxygen sensors. This can be attributed to the fast electrocatalytic ability for dissolved oxygen and to the efficiency of the electron transfer between oxygen and electrode.

The responses of common interference on the proposed sensor were also investigated. As can be seen in Table 1, in the PBS (pH 7.0) containing 30 μM dissolved oxygen at the applied potential of −300 mV, the responses caused by addition of 0.1 mM ascorbic acid, uric acid, 4-aminophenol, resorcinol, hydroquinone, Ca^{2+}, Na^+, NO_3^-, and SO_4^{2-} could be negligible (response ratio <5 %). This result is mainly due to the low working potential used in the determination of dissolved oxygen.

Table 1 The responses of common interference on the proposed sensor

Species added	Response ratio (%)
Ascorbic acid	4.1
Uric acid	2.9
4-Aminophenol	4.8
Resorcinol	3.9
Hydroquinone	4.3
Ca^{2+}	2.6
Na^+	1.8
NO_3^-	2.8
SO_4^{2-}	3.1

The reproducibility and long-term stability of the dendritic silver nanostructures modified GC electrode were examined as well. The device-to-device reproducibility was evaluated from the response to 30 μM dissolved oxygen at five electrodes independently, and the relative standard deviation was calculated to 3.1 %. Besides, the electrode was stored at 4 °C and measured every day, it retained about 86.2 % of its original sensitivity after 1 week.

4 Conclusions

In the present work, the dissolved oxygen sensor based on the three-dimensional silver dendrites modified GC electrode was prepared. This dendritic silver nanostructures synthesized by electrodeposition without any template or catalyst exhibited good electroreduction activity toward dissolved oxygen with high sensitivity and low detection limit. The efficient four-electron reaction of as-prepared sensor for dissolved oxygen reduction at a positively-shifted potential was also presented. Moreover, at a relatively low potential of −300 mV, the common interferences can be neglected. So, in conclusion, the current work showed a good potential for dissolved oxygen determination.

Acknowledgments The financial supports from National Natural Science Foundation of China (Grant No. 81127001) and Science and Technology Plan Project of Tianjin (Grant No. 11ZCGHHZ01300 and Grant No. 11ZCKFSY07000) are acknowledged.

References

1. Osborne PG, Li XF, Li YZ, Han HW (2001) Oxygen-sensing microdialysis probe for in vivo use. J Neurosci Res 63:224–232
2. Zagal JH, Gulppi M, Isaacs M, Cardenas-Jiron G, Aguirre MJ (1998) Linear versus volcano correlations between electrocatalytic activity and redox and electronic properties of metallophthalocyanines. Electrochim Acta 44:1349–1357
3. Komai Y (1998) Augmented respiration in a flying insect. J Exp Biol 201:2359–2366
4. Suzuki Y, Nishide H, Tsuchida E (2000) Membranes of the picket fence cobalt porphyrin complexed with poly(vinylimidazole and -pyridine)s: selective optical response to oxygen. Macromolecules 33:2530–2534
5. Bailey RT, Cruickshank FR, Deans G, Gillanders RN, Tedford MC (2003) Characterization of a fluorescent sol–gel encapsulated erythrosin B dissolved oxygen sensor. Anal Chim Acta 487:101–108
6. Freeman TM, Seitz WR (1981) Oxygen probe based on tetrakis(alkylamino)ethylene chemiluminescence. Anal Chem 53: 98–102
7. Clark LC (1956) Monitor and control of blood and tissue oxygen tensions. Trans Am Soc Artif Intern Organs 2:41–48
8. Martin CS, Dadamos TRL, Teixeira MFS (2012) Development of an electrochemical sensor for determination of dissolved oxygen by nickel-salen polymeric film modified electrode. Sens Actuators, B 175:111–117
9. Damos FS, Luz RCS, Tanaka AA, Kubota LT (2010) Dissolved oxygen amperometric sensor based on layer-by-layer assembly using host–guest supramolecular interactions. Anal Chim Acta 664:144–150
10. Santos LSS, Landers R, Gushikem Y (2011) Application of Manganese (II) phthalocyanine synthesized in situ in the SiO_2/SnO_2 mixed oxide matrix for determination of dissolved oxygen by electrochemical techniques. Talanta 85:1213–1216
11. Lin YH, Cui XL, Ye XR (2005) Electrocatalytic reactivity for oxygen reduction of palladium-modified carbon nanotubes synthesized in supercritical fluid. Electrochem Commun 7:267–274
12. Mao LQ, Arihara K, Sotomura T, Ohsaka T (2004) A novel alkaline air electrode based on a combined use of cobalt hexadecafluoro-phthalocyanine and manganese oxide. Electrochim Acta 49:2515–2521
13. Zhang MN, Yan YM, Gong KP, Mao LQ, Guo ZX, Chen Y (2004) Electrostatic layer-by-layer assembled carbon nanotube multilayer film and its electrocatalytic activity for O_2 reduction. Langmuir 20:8781–8785
14. Liu Y, Yan YL, Lei JP, Wu F, Ju HX (2007) Functional multiwalled carbon nanotube nanocomposite with iron picket-fence porphyrin and its electrocatalytic behavior. Electrochem Commun 9:2564–2570
15. El-Deab MS, Ohsaka T (2002) An extraordinary electocatalytic reduction of oxygen on gold nanoparticles-electrodeposited gold electrodes. Electrochem Commun 4:288–292
16. Cui HF, Ye JS, Zhang WD, Wang J, Sheu FS (2005) Electrocatalytic reduction of oxygen by a platinum nanoparticle/carbon nanotube composite electrode. J Electroanal Chem 577:295–302
17. Wei ZD, Chan SH, Li LL, Cai HF, Xia ZT, Sun CX (2005) Electrodepositing Pt on a nafion-bonded carbon electrode as a catalyzed electrode for oxygen reduction reaction. Electrochim Acta 50:2279–2287
18. Ye H, Crooks JA, Crooks RM (2007) Effect of particle size on the kinetics of the electrocatalytic oxygen reduction reaction catalyzed by Pt dendrimer-encapsulated nanoparticles. Langmuir 23:11901–11906
19. Kongkanand A, Kuwabata S (2003) Oxygen reduction at silver monolayer islands deposited on gold substrate. Electrochem Commun 5:133–137
20. Demarconnay L, Coutanceau C, Leger JM (2004) Electroreduction of dioxygen (ORR) in alkaline medium on Ag/C and Pt/C nanostructured catalysts—effect of the presence of methanol. Electrochim Acta 49:4513–4521
21. Lu YZ, Wang YC, Chen W (2011) Silver nanorods for oxygen reduction: strong effects of protecting ligand on the electrocatalytic activity. J Power Sour 196:3033–3038
22. Ahmadi TS, Wang ZL, Green TC, Henglein A, El-sayed MA (1996) Shape-controlled synthesis of colloidal platinum nanoparticles. Science 272:1924–1925
23. Ju HX, Shen CZ (2001) Electrocatalytic reduction and determination of dissolved oxygen at a poly(nile blue) modified electrode. Electroanalysis 13:8–9
24. Qin X, Wang H, Wang X, Miao Z, Fang Y, Chen Q, Shao X (2011) Synthesis of dendritic silver nanostructures and their application in hydrogen peroxide electroreduction. Electrochim Acta 56:3170–3174
25. Wen XG, Xie YT, Mak MWC, Cheung KY, Li XY, Renneberg R, Yang S (2006) Dendritic nanostructures of silver: facile synthesis, structural characterizations, and sensing applications. Langmuir 22:4836–4842
26. Wei GD, Nan CW, Deng Y, Lin YH (2003) Self-organized synthesis of silver chainlike and dendritic nanostructures via a solvothermal method. Chem Mater 15:4436–4441
27. Glasspool W, Atkinson J (1998) A screen-printed amperometric dissolved oxygen sensor unilising an immobilised electrolyte gel and membrane. Sens Actuators, B 48:308–317
28. Andrieux CP, Savéant JM (1978) Heterogenous (chemically modified electrodes, polymer electrodes) vs. homogeneous catalysis of electrochemical reactions. J Electroanal Chem 93:163–168
29. Xiao X, Zhou B, Tan L, Tang H, Zhang Y, Xie Q, Yao S (2011) Poly(methylene blue) doped silica nanocomposites with cross-linked cage structure: electropolymerization, characterization and catalytic activity for reduction of dissolved oxygen. Electrochim Acta 56:10055–10063
30. Damos FS, Luz RCS, Tanaka AA, Kubota LT (2010) Dissolved oxygen amperometric sensor based on layer-by-layer assembly using host–guest supramolecular interactions. Anal Chim Acta 664:144–150
31. Luz RCS, Damos FS, Tanaka AA, Kubota LT (2006) Dissolved oxygen sensor based on cobalt tetrasulphonated phthalocyanine immobilized in poly-L-lysine film onto glassy carbon electrode. Sens Actuators, B 114:1019–1027